Proceedings of CONF-MCEE 2026 Symposium: Advances in Sustainable Aviation and Aerospace Vehicle Automation
DOI: 10.54254/2755-2721/2026.KA29319

Research Progress on Electron-Type 122 Iron-Based Superconductors

Peiyuan Wang

QianWeiChang College, Shanghai University, Shanghai, China
wangpeiyuan@shu.edu.cn

Abstract. Owing to their high superconducting transition temperature (Tc), large upper critical field (Hc_2), high critical current density (Jc), and excellent crystalline stability, electron-type 122 iron-based superconductors have become a focal point of research. This paper first reviews the development and classification of iron-based superconductors, then summarizes how electron doping tunes Tc and discusses key physical characteristics such as quantum-critical behavior and the competition between nematic order and superconductivity. It next surveys advances in materials synthesis—including single-crystal growth, defect engineering, and heterostructure design—and examines progress on mechanisms involving spin fluctuations and Fermi-surface evolution. Finally, it outlines prospects for future research in this family.

Keywords: Iron-based superconductor, (La, Na, K)Fe_2As_2, electron-doped

1. Introduction

Superconductivity, one of the most important macroscopic quantum phenomena in condensed-matter physics, is characterized by zero electrical resistance, perfect diamagnetism, and macroscopic quantum effects. When the temperature falls below a critical value Tc, a superconductor's resistivity drops abruptly to zero, allowing lossless current transport—its defining zero-resistance property. In addition, upon penetration of an external magnetic field, the magnetic induction decays exponentially inside a superconductor, yielding zero internal magnetic flux density—this is the Meissner effect, i.e., perfect diamagnetism [1]. Superconducting materials have significant application value in energy, transportation, medicine, and large-scale scientific infrastructure. With technological advances, superconductivity has been adopted in high-end instrumentation such as MRI systems and NMR spectrometers, in large science projects including high-energy accelerators and fusion devices, and in power equipment and maglev transport. The demand for superconducting materials and their technologies is thus increasingly urgent; developing high-performance superconductors and applications is of great economic and societal significance.

By composition, known superconductors include conventional metallic and alloy superconductors, cuprate high-temperature superconductors, fullerides and related compounds, iron-based superconductors, and several other families [2]. Compared with conventional low-temperature metallic superconductors, the iron-based superconductors discovered in 2008 exhibit higher Tc and Hc_2 and are regarded as practical candidates for high-field applications [3]—particularly in

© 2025 The Authors. This is an open access article distributed under the terms of the Creative Commons Attribution License 4.0 (https://creativecommons.org/licenses/by/4.0/).

DOI: 10.54254/2755-2721/2026.KA29319

accelerators, high-field MRI, and controlled fusion—owing to their distinctive advantages. Relative to the cuprates, iron-based superconductors possess longer coherence lengths and weaker anisotropy, and they are not brittle copper-oxide ceramics. Thus, iron-based materials bridge the gaps between conventional metals and cuprates and hold strong development prospects. The principal iron-based families include 1111 (ZrCuSiAs-type), 122 ($ThCr_2Si_2$-type), 111 (PbFCl-type), 11 (PbO-type), and variants [4].

Within these, AFe_2As_2 (A=Ca, Sr, Ba) compounds—i.e., the electron-type 122 family—offer more stable crystal structures and greater chemical inertness, with lower sensitivity to air and moisture; some members also have large Hc and high Jc. Compared with other iron-based families, 122 compounds yield large, high-quality single crystals more readily. Owing to their experimental utility and application promise, they have been widely studied.

This article reviews the development and basic characteristics of iron-based superconductors; outlines their classification and distinctive properties; provides a detailed summary of advances specific to electron-type 122 compounds; and concludes with an outlook on future directions.

2. Iron-based superconductors

2.1. Historical development

Superconductivity was first discovered in 1911, when Kamerlingh Onnes cooled elemental Hg with liquid helium and observed that its resistance vanished abruptly at about 4.2 K—launching the modern study of superconductivity. Superconductivity was subsequently observed in many elements and alloys, though Tc was low for typical metals such as Hg, Pb, and Nb. In 1957, Bardeen, Cooper, and Schrieffer formulated the BCS theory of superconductivity. In 1986, Bednorz and Müller discovered superconductivity at 36 K in the La-Ba-Cu-O system [5], marking the advent of high-temperature superconductivity; Tc was then further raised in YBaCuO, BiSrCaCuO, and other cuprates. In the 21st century, MgB_2 (39 K—the highest Tc among conventional superconductors), iron-based (2006 onward), and nickel-based (2019) superconductors were identified [6]. Pressure and chemical doping have been widely employed to enhance Tc[6b], opening new avenues for research. Figure 1 sketches key milestones.

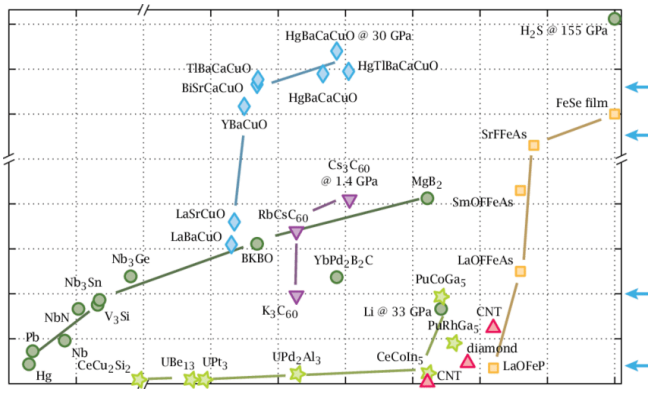

Figure 1. Historical development of selected superconductors [7]

2.2. Classification of iron-based superconductors

Despite encompassing hundreds of compounds, iron-based superconductors share a layered crystal motif. The essential structural element is a two-dimensional Fe–X conducting layer (X = As, Se, S,

DOI: 10.54254/2755-2721/2026.KA29319

etc.), where Fe^{2+} ions form tetrahedral coordination with pnictogens or chalcogens. These Fe–X layers stack along the crystallographic c-axis, and superconductivity mainly resides within them. Inserting different structural blocks between layers yields distinct crystal architectures, giving rise to four principal families:

(1) 1111 family: RFeAsO (R = rare earth such as La, Sm).

La_2O_2 layers are intercalated between Fe_2As_2 layers, wherein each Fe atom is surrounded by four As atoms in the Fe_2As_2 layers, while each O atom is surrounded by four La atoms in the La_2O_2 layers [8]. the structure is ZrCuSiAs-type (space group P4/nmm) [9]. Shortly after LaOFeAs, replacing La with Sm produced $SmFeAsO_{1-x}F_x$ (x=0.15) with Tc=43 K [10], the first iron-based superconductor to surpass the McMillan limit (39 K).

(2) 111 family: MFeAs (M=alkali metal).

Single FeAs layers are separated by M^+ ions (e.g., Li^+, Na^+). These compounds can be superconducting without extrinsic doping. They adopt the PbFCl-type structure (P4/nmm); examples include LiFeAs [11], NaFeAs [12], and LiFeP [13].

(3) 11 family: FeX (X = Se, Te).

No interlayer cations are present; the structure comprises single or multiple FeX layers (FeSe is tetragonal; FeTe forms a distorted multilayer) [14]. The structure is anti-PbO tetragonal (P4/nmm) [15]. The structural simplicity facilitates exploration of intrinsic properties and the growth of large, high-quality single crystals amenable to spectroscopic, transport, and optical probes.

(4) 122 family: AFe_2As_2 (A=alkaline-earth metal such as Ba, Sr).

FeAs layers appear as bilayers separated by A^{2+} ions; ionic radius tunes interlayer spacing and structural distortion. The structure is $ThCr_2Si_2$-type (I4/mmm) [16]. Superconductivity can be tuned by electron doping (e.g., Co substitution on Fe in $BaFe_2As_2$) or hole doping (e.g., K substitution on $SrFe_2As_2$); Tc can be high in certain compositions. Owing to its clear layered framework and sensitive doping response, the 122 family is a model platform for electron-type iron-based superconductivity and is the focus here.

2.3. Distinctive properties

Iron-based superconductors generally possess quasi-two-dimensional structures comprising superconducting FeX layers interleaved by spacer layers (except the 11 family, which lacks spacers). The weak interlayer coupling results in pronounced in-plane vs. out-of-plane anisotropy in transport and mechanics; in-plane conductivity greatly exceeds interlayer conductivity, and superconducting transport and Jc differ markedly between in-plane and c-axis directions.

A striking feature is the coexistence of magnetism (arising from unpaired 3d electrons of Fe^{2+}) with superconductivity's perfect diamagnetism—an unusual combination. Parent compounds typically exhibit antiferromagnetic long-range order that is suppressed by carrier doping (electrons or holes), upon which superconductivity emerges. This differs from conventional electron–phonon superconductors and from cuprates, whose parents are insulators.

3. Research progress on electron-type 122 iron-based superconductors

3.1. Developmental overview

Electron doping commonly involves substituting transition metals such as Co or Ni for Fe, introducing extra electrons and increasing carrier concentration to promote superconductivity.

DOI: 10.54254/2755-2721/2026.KA29319

In 2008, Co doping in $BaFe_2As_2$ yielded single crystals $BaFe_{1.8}Co_{0.2}As_2$ with Tc=22 K—the first electron-doped 122 case following multiple hole-doped successes [17]. Subsequent work showed an 8% Co composition produced a very narrow transition width (~0.6 K), much smaller than in F- or K-doped systems, indicating more homogeneous electron doping; magnetic susceptibility reached full diamagnetism ($4\pi\chi\approx-1$), confirming bulk superconductivity [18]. In 2011, rare-earth doping in $CaFe_2As_2$ achieved Tc=49 K [19]—well above the ~38 K ceiling in hole-doped 122 systems—representing the first electron-doped superconductivity in Ca122.

Other substitutions on Fe and As sites soon followed. In 2009, Ni doping produced $BaFe_{2-x}Ni_xAs_2$ crystals with Tc up to 20.5 K at x=0.096, with narrower transitions than Co-doped analogues [20]. Using 4d/5d dopants (Rh, Ir, Pd) in $SrFe_2As_2$ yielded peak Tc values of 21.9 K, 24.2 K, and 8.7 K, respectively [21]. Also in 2009, isovalent P substitution at the As site induced superconductivity in $EuFe_2(As_{0.7}P_{0.3})_2$ with Tc = 26 K coexisting with Eu_{2+} ferromagnetism at 20 K [22]—a rare platform to probe the interplay between superconductivity and ferromagnetism.

Building on this, studies of $BaFe_{2-x}Ni_xAs_2$ revealed that long-range commensurate antiferromagnetism (C-AF) does not coexist with the superconducting state; near optimal doping, C-AF gives way to short-range incommensurate AF (IC-AF), which coexists and directly competes with superconductivity. No conventional magnetic quantum critical point appears at optimal doping. Further work showed that structural and AF orders converge toward a quantum bicritical point but that the emergent IC-AF phase avoids true criticality; strong magnetoelastic coupling is key in tuning phase transitions, with secondary order steering deviations from ideal quantum-critical behavior [23].

3.2. Recent advances

In recent years, besides research focusing on critical temperature (Tc), upper critical field (Hc), and critical current density (Jc), the electron-doped 122 system has two major key issues: first, its high-temperature superconductivity mechanism has not yet been fully clarified, and second, the interaction mechanism between magnetism and superconductivity needs further exploration. Researchers have carried out extensive investigations around these two issues. Beyond intrinsic physical properties such as electronic states and nematic order, certain progress has also been made in the thermodynamic properties and optical properties of superconducting materials.

3.2.1. Single-crystal growth and thin-film fabrication

The growth and doping control of iron-based 122 system single crystals serve as the foundation for studying their superconducting characteristics. The core lies in optimizing growth methods to obtain high-purity, large-sized crystals while achieving precise regulation of dopant concentration and homogeneity. The primary single-crystal growth techniques for this system are the flux method and optical floating-zone growth.

In the flux method, self-fluxes including FeAs, CaAs, and NaAs are widely utilized. For instance, in 2014, Zhang et al. from the Institute of Physics, Chinese Academy of Sciences (IOP, CAS) grew $BaFe_{2-x-y}Ni_xCr_yAs_2$ single crystals using FeAs self-flux. After melting at 1180 °C, the system was cooled at a rate of 5 °C/h to 1050 °C, followed by quenching, resulting in crystals with a size of up to 15 mm [24]. In 2017, Xie et al. employed CaAs as the flux; after melting at 1180 °C, the system was cooled at 3 °C/h, successfully preparing 6 mm-scale $Ca_{1-y}La_yFe_{1-x}Ni_xAs_2$ single crystals [25]. In 2018, the Gu group used NaAs and NaF as fluxes, and serendipitously obtained millimeter-scale $La_{0.34}Na_{0.66}Fe_2As_2$ single crystals during the growth of $LaFeAsO_{1-y}F_y$; these crystals could be

DOI: 10.54254/2755-2721/2026.KA29319

separated via water-soluble flux [26].In 2022, Zhou et al. adopted the NaAs-flux method: after melting at 1150 °C, the system was cooled at 2 °C/h, yielding $Ca_{1-x}Na_xFe_2As_2$ single crystals larger than 10 mm [27]. The optical floating-zone method is suitable for easily decomposable systems. For example, the Liu group from the Max Planck Institute for Solid State Research, Germany, grew $KxFe_{2-y}Se_2$ single crystals under 8 bar argon atmosphere at a rate of 1.0 mm/h. End-quenching was applied to mitigate decomposition, ultimately obtaining single crystals of approximately 6×10 mm [28].

Dopant control relies on precise characterization and process optimization. Various research groups have used Inductively Coupled Plasma (ICP) and Energy Dispersive X-ray Spectroscopy (EDX) to characterize dopant homogeneity. For instance, the IOP, CAS team measured the segregation coefficients of Ni and Cr in $BaFe_{2-x-y}Ni_xCr_yAs_2$ as 0.82±0.10 and 0.68±0.11, respectively; in Ca1-yLayFe1-xNixAs2, they found that the actual Ni dopant content was 0.8 times the nominal value [24]. The Luo group from the University of Science and Technology of China (USTC) noted that the flux method is suitable for large-sized single crystals, the floating-zone method is applicable to labile phases, and post-growth annealing can improve dopant homogeneity [29].

3.2.2. New compound systems and structures

In 2017, a research team led by M. Moroni at the University of Pavia, Italy, irradiated $Ba(Fe_{1-x}Rh_x)_2As_2$ with 5.5 MeV protons to introduce defects [30]. By combining resistivity and ^{75}AsNMR techniques, they investigated the effects of irradiation on superconductivity and spin fluctuations in the normal state. The study found that proton irradiation only slightly suppressed the superconducting transition temperature Tc (for the sample with x=0.068, Tc decreased from 23.3 K to 21.3 K), but significantly altered the spin characteristics in the normal state (for the sample with x=0.068, the spin correlation switched from antiferromagnetic to ferromagnetic). The irradiation-induced defects enhanced the activation energy of low-frequency spin fluctuations and slowed down fluctuations between nematic phases at (0,π) and (π,0). This indicates that non-magnetic defects have a substantial influence on spin correlations in iron-based superconductors, while their effect on superconductivity is weaker than that of crystalline structure modulation.

In 2019, the Iyo team from the National Institute of Advanced Industrial Science and Technology (AIST), Japan, employed a cubic-anvil high-pressure apparatus, using LaAs and Fe_2As as starting materials [31]. Under 3.4 GPa pressure and 960 °C, heated for 1.5 h and then rapidly quenched, they obtained the collapsed tetragonal phase $LaFe_2As_2$ (La122). La122 possesses two crystal phases: the uncollapsed (superconducting) phase (UT) and the collapsed (non-superconducting) phase (CT). This was the first instance of a heavily electron-doped 122-type iron-based superconductor synthesized under high pressure, which was of great significance. In the same year, research teams from Shimane University and Osaka University investigated the electronic structure of $LaFe_2As_2$[32]. Although first-principles calculations showed an absence of hole Fermi surfaces near the Γ point, comparison of band structures, Fermi surfaces (FS), and densities of states between the UT and CT phases—while hypothetically removing the contribution of La d orbitals—revealed that a hole Fermi surface essentially exists near the Γ point in the uncollapsed phase. In the non-superconducting collapsed phase, the hole Fermi surface disappears. The difference between the two phases can be reasonably explained by a spin-fluctuation-mediated pairing mechanism.

Since La122 broke the established rule that superconductivity vanishes when doping exceeds 0.2e/Fe in iron-based superconductors, I.I. Mazin's team at the U.S. Naval Research Laboratory conducted a detailed study of its physical properties [33]. They found that in the two crystal phases

DOI: 10.54254/2755-2721/2026.KA29319

of La122, the UT phase exhibited disordered magnetic moments, whereas the CT phase was locally non-magnetic. The valence state of La was +2.6 to +2.7 (rather than +3), reducing the effective Fe doping level to 0.30–0.35e/Fe. Although overdoped, this was lower than the apparent value of 0.5e and closer to the doping range of conventional iron-based superconductors. Calculations of exchange interactions and non-interacting susceptibility both confirmed that the traditional spin-fluctuation-mediated superconducting mechanism is applicable to this system.

In a magnetic field, superconductors form a "vortex state," where carriers circulate around magnetic flux lines. Free motion of vortices reduces the current-carrying capacity of the superconductor. Therefore, in addition to elemental doping, vortex motion can be suppressed by artificially introducing pinning centers through particle irradiation, thereby enhancing the current-carrying capacity of the material. In 2020, Nazir et al. employed pulsed laser deposition (PLD) to grow $BaFe_{1.84}Co_{0.16}As_2$ thin films on CaF_2 (00l) substrates, and subsequently irradiated them at room temperature with 600 keV He+ ions. At a fluence of 5×10^{13} cm−2, the critical current density Jc reached its maximum: under 4.5 K and 1 T, Jc reached 2.4 MA·cm−2, about five times higher than in unirradiated samples [34]. Pinning force analysis showed that the irradiation introduced pinning centers of the same type as in unirradiated samples, still dominated by planar defects. This result provides experimental evidence for optimizing electron-doped 122-type iron-based superconductors via low-energy light-ion irradiation.

In June 2025, a research team from the State Key Laboratory of Low-Dimensional Quantum Physics, Tsinghua University, employed molecular beam epitaxy (MBE) to fabricate $Ba(Fe_{1-x}Co_x)_2As_2$ (BFCA) epitaxial films on $SrTiO_3$ (001) substrates, growing a BaAs monolayer (different from the conventional electron-doped $BaFe_{2-x}Co_x$ structure) and constructing a high-crystallinity BaAs/BFCA heterostructure. This heterostructure system exhibited minimal disorder effects, approaching the clean limit. Moreover, the study found that the energy gap remained stable with variations in BFCA thickness, and superconductivity could be tuned via Co doping. Deviations from optimal doping reduced the gap, revealing the carrier-regulation behavior [35]. This work addresses the issue of chemical-disorder interference in the exploration of high-temperature superconducting pairing mechanisms. By leveraging two-dimensional interfaces, it offers a new pathway to reveal intrinsic properties and provides direct experimental evidence for the unconventional superconducting mechanism of iron-based superconductors.

3.2.3. Intrinsic physical properties and correlated quantum phenomena

In 2016, Derondeau et al. employed a fully relativistic Dirac formalism to investigate the hyperfine field Bhf of the $BaFe_2As_2$ family and its relation to magnetic moments [36]. The results showed that the hyperfine field of electron-doped $Ba(Fe_{1-x}Co_x)_2As_2$ and $Ba(Fe_{1-x}Ni_x)_2As_2$ strongly depends on both the doping type and the concentration x. At the same time, the average magnetic moment μavg in electron-doped systems (Co-122 and Ni-122) decreases with increasing concentration until the antiferromagnetic order collapses at the critical concentration xcrit, with Bhf exhibiting a similar trend. Therefore, correlating Bhf with the average magnetic moment μ of the compound is unreasonable, which differs from earlier literature.

In iron-based superconductors, spin-density-wave (SDW) magnetic order is suppressed by doping, and unconventional superconductivity emerges near SDW instabilities [37]. In 2016, teams from the Center for High Pressure Science and Technology Advanced Research and the Institute of Physics, Chinese Academy of Sciences, carried out a detailed temperature-dependent optical response study on electron-doped Ba122 systems. By analyzing the reflectivity and optical conductivity of Co-doped Ba122 samples at different temperatures, they found that as Co doping

DOI: 10.54254/2755-2721/2026.KA29319

increased, the onset temperature of SDW fluctuations was suppressed. In addition, the suppression of low-frequency conductivity and the transfer of spectral weight occurred at temperatures far above the SDW transition temperature. These results indicate a close relationship between magnetic order and nematic order.

In 2018, Matusiak et al. measured the in-plane anisotropy of the Seebeck coefficient, Nernst coefficient, and resistivity in a series of detwinned $Ba(Fe_{1-x}Co_x)_2As_2$ single crystals. They observed that the Hall coefficient of these samples exhibited a step-like anomaly at the structural/magnetic transition temperature Ttr, which was used to determine Ttr for different doping levels [38]. In the optimally doped sample (x=0.06), although no long-range magnetic order was detected, in-plane anisotropy in transport properties still appeared below T≈120 K. However, this anisotropy was smaller, and the differences in the Seebeck and Nernst coefficients along and perpendicular to the uniaxial strain direction had opposite signs compared to those in underdoped crystals with x=0.024 and 0.045. For these underdoped samples, the Nernst anisotropy was insensitive to the SDW transition, suggesting that the origin of nematicity may not be magnetic in nature.

In 2019, the team of Straquadine at Stanford University and the U.S. National High Magnetic Field Laboratory (NHMFL) modified the conventional elastoresistivity technique (commonly used to probe electronic nematic fluctuations) [39]. They suppressed superconductivity in $Ba(Fe_{0.926}Co_{0.074})_2As_2$ single crystals with higher magnetic fields and measured the elastoresistivity coefficient (as a proxy for nematic susceptibility) in the normal state at 1.2 K using a 65 T pulsed magnet. The results showed that, in the field-induced normal state, nematic susceptibility increased monotonically with decreasing temperature, consistent with the existence of a quantum critical point near this composition. At the same time, no significant field dependence of elastoresistivity was observed, indicating that extreme magnetic fields did not substantially alter the driving force behind nematic fluctuations.

In 2022, a research team led by Wuttke at the Leibniz Institute for Solid State and Materials Research demonstrated that the Nernst coefficient can be used to probe electronic nematic fluctuations. They measured the Nernst coefficient (ν) of Rh-doped Ba122 superconductors over a wide temperature range (5–300 K) and high magnetic fields (14 T), analyzing the variation of ν/T (Nernst coefficient divided by temperature) with doping and temperature in the normal state (above Tc). The study found that the Nernst coefficient, particularly ν/T, is highly sensitive to electronic nematic fluctuations and does not require applied lattice strain, making it an effective probe of nematic fluctuations. Furthermore, the study revealed that the Nernst effect directly reflects electronic states (Fermi surface distortions), in contrast to elastoresistivity, which depends on electron-lattice coupling mechanisms [40].

3.2.4. Advances in pairing-mechanism studies

Ultrafast THz pump–probe spectroscopy on $Ba(Fe_{1-x}Co_x)_2As_2$ reveals photoinduced nonequilibrium pair breaking and excitonic-like states; underdoped samples (x=0.047) require lower energy for the SC–normal transition than overdoped ones, offering fresh constraints on pairing dynamics [41].

The role of nematic fluctuations remains debated. Inelastic x-ray scattering on underdoped and optimally doped $Ba(Fe_{1-x}Co_x)_2As_2$ shows anomalous softening of acoustic phonons and a nematic correlation length ξ following a power law $(T-T_0)^{-1/2}$ over a broad temperature range [42]—consistent with Curie–Weiss-like nematic susceptibility seen earlier in FeSe [43]—and indicative of mean-field character. Nematic–elastic coupling extends fluctuation effects well above Ts and competes with superconductivity. Combining anisotropic strain with Raman scattering in $Ba(Fe_{1-x}Co_x)_2As_2$ further isolates nematic from magnetic fluctuations, demonstrating that Tc variations track

DOI: 10.54254/2755-2721/2026.KA29319

nematic fluctuations, which contribute significantly to pairing—consistent with theoretical expectations of enhanced Tc near a nematic quantum critical point.

In 2022, the Philippe group from the University of Paris Cité focused on $Ba(Fe_{1-x}Co_x)_2As_2$ — the prototypical electron-doped 122 system — as their research subject. By combining anisotropic strain and Raman scattering techniques, they successfully distinguished the effects of magnetic fluctuations and nematic fluctuations on the critical superconducting transition temperature (Tc) [44].The study found that in this system, the variation of Tc is closely related to nematic fluctuations: nematic fluctuations make a significant contribution to electron pairing, which verifies the theory of Tc enhancement near the nematic quantum critical point(NQCP).

4. Conclusions and outlook

This review has surveyed the electron-type 122 iron-based superconductors. After recapping the broader development and classification of iron-based materials, we emphasized the 122 family as an ideal platform for studying electron-doping effects due to its clear layered structure and ease of single-crystal growth. We summarized how substituting transition metals (Co, Ni, Rh, etc.) on Fe effectively tunes Tc, and we discussed salient physics, including avoided quantum criticality, magnetoelastic coupling, and the competition between nematic and superconducting orders. We also highlighted progress in crystal growth, defect engineering (e.g., proton/ion irradiation), heterostructure design (e.g., BaAs/BFCA interfaces), and mechanism-oriented studies of spin fluctuations and Fermi-surface evolution.

Despite rich physics and promising potential, two core challenges remain. First, the microscopic mechanism of high-temperature superconductivity is not yet fully established, especially the quantitative roles of spin and nematic fluctuations in pairing. Second, relative to hole-doped 122 conductors—which already deliver high transport Jc in practical tapes—electron-doped counterparts lag in vortex-pinning optimization and high-field application studies. Future efforts should focus on: (1) combining advanced spectroscopies with theory to determine pairing symmetry and correlation effects; (2) refining doping control and defect introduction to engineer optimized pinning landscapes and enhance current-carrying capacity; (3) exploring new electron-type compounds and clean heterostructures to broaden materials space and tuning dimensions; and (4) pushing fabrication and performance of electron-type 122 wires and tapes to close the gap in power and magnet applications.

References

[1] F. Steglich, J. Aarts, C. D. Bredl, W. Lieke, D. Meschede, W. Franz, H. Schäfer, Physical Review Letters 1979, 43, 1892-1896.
[2] C. Rial, E. Morán, M. A. Alario-Franco, U. Amador, N. H. Andersen, Physica C: Superconductivity 1995, 254, 233-248.
[3] L. Taillefer, Annual Review of Condensed Matter Physics 2010, 1, 51-70.
[4] S. Tan, Y. Zhang, M. Xia, Z. Ye, F. Chen, X. Xie, R. Peng, D. Xu, Q. Fan, H. Xu, J. Jiang, T. Zhang, X. Lai, T. Xiang, J. Hu, B. Xie, D. Feng, Nature Materials 2013, 12, 634-640.
[5] J. G. Bednorz, K. A. Müller, Zeitschrift für Physik B Condensed Matter 1986, 64, 189-193.
[6] aH.-H. Wen, S. Li, Annual Review of Condensed Matter Physics 2011, 2, 121-140; bT. Watanabe, H. Yanagi, T. Kamiya, Y. Kamihara, H. Hiramatsu, M. Hirano, H. Hosono, Inorganic Chemistry 2007, 46, 7719-7721.
[7] P. Ray, 2015.
[8] Y. Kamihara, T. Watanabe, M. Hirano, H. Hosono, J Am Chem Soc 2008, 130, 3296-3297.
[9] Y. Kamihara, T. Watanabe, M. Hirano, H. Hosono, Journal of the American Chemical Society 2008, 130, 3296-3297.
[10] X. H. Chen, T. Wu, G. Wu, R. H. Liu, H. Chen, D. F. Fang, Nature 2008, 453, 761-762.

DOI: 10.54254/2755-2721/2026.KA29319

[11] X. C. Wang, Q. Q. Liu, Y. X. Lv, W. B. Gao, L. X. Yang, R. C. Yu, F. Y. Li, C. Q. Jin, Solid State Communications 2008, 148, 538-540.
[12] R. Cortes-Gil, S. J. Clarke, Chemistry of Materials 2011, 23, 1009-1016.
[13] Z. Deng, X. C. Wang, Q. Q. Liu, S. J. Zhang, Y. X. Lv, J. L. Zhu, R. C. Yu, C. Q. Jin, Europhysics Letters 2009, 87, 37004.
[14] A. Leithe-Jasper, W. Schnelle, C. Geibel, H. Rosner, Physical Review Letters 2008, 101, 207004.
[15] F.-C. Hsu, J.-Y. Luo, K.-W. Yeh, T.-K. Chen, T.-W. Huang, P. M. Wu, Y.-C. Lee, Y.-L. Huang, Y.-Y. Chu, D.-C. Yan, M.-K. Wu, Proceedings of the National Academy of Sciences 2008, 105, 14262-14264.
[16] J. Guo, S. Jin, G. Wang, S. Wang, K. Zhu, T. Zhou, M. He, X. Chen, Physical Review B 2010, 82, 180520.
[17] A. S. Sefat, R. Jin, M. A. McGuire, B. C. Sales, D. J. Singh, D. Mandrus, Physical Review Letters 2008, 101, 117004.
[18] A. S. Sefat, D. J. Singh, R. Jin, M. A. McGuire, B. C. Sales, F. Ronning, D. Mandrus, Physica C: Superconductivity 2009, 469, 350-354.
[19] C. Chu, EPJ Web of Conferences 2012, 23, 00004.
[20] L. J. Li, Y. K. Luo, Q. B. Wang, H. Chen, Z. Ren, Q. Tao, Y. K. Li, X. Lin, M. He, Z. W. Zhu, G. H. Cao, Z. A. Xu, New Journal of Physics 2009, 11, 025008.
[21] F. Han, X. Zhu, P. Cheng, G. Mu, Y. Jia, L. Fang, Y. Wang, H. Luo, B. Zeng, B. Shen, L. Shan, C. Ren, H.-H. Wen, Physical Review B 2009, 80, 024506.
[22] Z. Ren, Q. Tao, S. Jiang, C. Feng, C. Wang, J. Dai, G. Cao, Z. a. Xu, Physical Review Letters 2009, 102, 137002.
[23] X. Lu, H. Gretarsson, R. Zhang, X. Liu, H. Luo, W. Tian, M. Laver, Z. Yamani, Y.-J. Kim, A. H. Nevidomskyy, Q. Si, P. Dai, Physical Review Letters 2013, 110, 257001.
[24] R. Zhang, D. Gong, X. Lu, S. Li, P. Dai, H. Luo, Superconductor Science and Technology 2014, 27.
[25] T. Xie, D. Gong, W. Zhang, Y. Gu, Z. Huesges, D. Chen, Y. Liu, L. Hao, S. Meng, Z. Lu, S. Li, H. Luo, Superconductor Science and Technology 2017, 30, 095002.
[26] Y. Gu, J.-O. Wang, X. Ma, H. Luo, Y. Shi, S. Li, Superconductor Science and Technology 2018, 31, 125008.
[27] H.-L. Zhou, Y.-H. Zhang, Y. Li, S.-L. Li, W.-S. Hong, H.-Q. Luo, Chinese Physics B 2022, 31, 117401.
[28] Y. Liu, Z. C. Li, W. P. Liu, G. Friemel, D. S. Inosov, R. E. Dinnebier, Z. J. Li, C. T. Lin, Superconductor Science and Technology 2012, 25, 075001.
[29] X. Luo, X. Chen, Science China Materials 2015, 58, 77-89.
[30] M. Moroni, L. Gozzelino, G. Ghigo, M. A. Tanatar, R. Prozorov, P. C. Canfield, P. Carretta, Physical Review B 2017, 96, 094523.
[31] A. Iyo, S. Ishida, H. Fujihisa, Y. Gotoh, I. Hase, Y. Yoshida, H. Eisaki, K. Kawashima, The Journal of Physical Chemistry Letters 2019, 10.
[32] H. Usui, K. Kuroki, Physical Review Research 2019, 1, 033025.
[33] I. I. Mazin, M. Shimizu, N. Takemori, H. O. Jeschke, Physical Review Letters 2019, 123, 267001.
[34] M. Nazir, Z. Xu, N. H. Peng, N. Akhtar, P. Papakonstantinou, R. P. Webb, Y. Ma, D. Zheng, Superconductor Science and Technology 2020, 33, 075012.
[35] M.-Q. Ren, Q.-J. Cheng, H.-H. He, Z.-X. Deng, F.-J. Cheng, Y.-W. Wang, C.-C. Lou, Q. Zhang, L. Gu, K. Liu, X.-C. Ma, Q.-K. Xue, C.-L. Song, Physical Review Letters 2025, 134, 246203.
[36] G. Derondeau, J. Minár, H. Ebert, Physical Review B 2016, 94, 214508.
[37] B. Xu, Y. M. Dai, H. Xiao, B. Shen, Z. R. Ye, A. Forget, D. Colson, D. L. Feng, H. H. Wen, X. G. Qiu, R. P. S. M. Lobo, Physical Review B 2016, 94, 085147.
[38] M. Matusiak, K. Rogacki, T. Wolf, Physical Review B 2018, 97, 220501.
[39] J. A. W. Straquadine, J. C. Palmstrom, P. Walmsley, A. T. Hristov, F. Weickert, F. F. Balakirev, M. Jaime, R. McDonald, I. R. Fisher, Physical Review B 2019, 100, 125147.
[40] C. Wuttke, F. Caglieris, S. Sykora, F. Steckel, X. Hong, S. Ran, S. Khim, R. Kappenberger, S. L. Bud'ko, P. C. Canfield, S. Wurmehl, S. Aswartham, B. Büchner, C. Hess, npj Quantum Materials 2022, 7, 82.
[41] X. Yang, L. Luo, M. Mootz, A. Patz, S. L. Bud'ko, P. C. Canfield, I. E. Perakis, J. Wang, Physical Review Letters 2018, 121, 267001.
[42] A. M. Merritt, F. Weber, J. P. Castellan, T. Wolf, D. Ishikawa, A. H. Said, A. Alatas, R. M. Fernandes, A. Q. R. Baron, D. Reznik, Physical Review Letters 2020, 124, 157001.
[43] A. E. Böhmer, P. Burger, F. Hardy, T. Wolf, P. Schweiss, R. Fromknecht, M. Reinecker, W. Schranz, C. Meingast, Phys Rev Lett 2014, 112, 047001.
[44] J.-C. Philippe, A. Lespinas, J. Faria, A. Forget, D. Colson, S. Houver, M. Cazayous, A. Sacuto, I. Paul, Y. Gallais, Physical Review Letters 2022, 129, 187002.